Case Studies in Thermal Engineering 49 (2023) 103357

Contents lists available at ScienceDirect

Case Studies in Thermal Engineering

journal homepage: www.elsevier.com/locate/csite

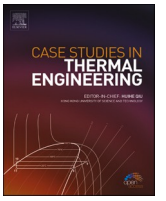

Two phase simulation of solar still in the presence of phase change materials in its bottom and aluminum nanoparticles in the water

Jawed Mustafa [a,**], Saeed Alqaed [a], Mohsen Sharifpur [b,c,*]

[a] Mechanical Engineering Department, College of Engineering, Najran University, P.O. Box (1988), Najran, 61441, Saudi Arabia
[b] Department of Mechanical and Aeronautical Engineering, University of Pretoria, South Africa
[c] Department of Medical Research, China Medical University Hospital, China Medical University, Taichung, Taiwan

ARTICLE INFO

Handling Editor: Huihe Qiu

Keywords:
Nanoparticles
Numerical method
PCM
Water desalination
Two-phase mixture

ABSTRACT

This article performs a numerical study on a transient solar still (SOST) by utilizing a variable heat flux using COMSOL software. A phase change material (PCM) layer with a thickness of 10–50 mm is placed at the bottom of the desalination. Some aluminum nanoparticles are added to the water in the water desalination, and the two-phase method is used to simulate this part of the desalination water. Other variables include the angle of the glass that changes from 10 to 45° and the heat transfer coefficient (HTFC) on the glass that varies from 5 to 300 W/m^2. The effect of these variables on the average PCM temperature (T-PCM), PCM volume fraction (VOF-PCM), average moisture (AV-MO) temperature, and AV-MO concentration is examined in 12 h. The simulations are done using the finite element method (FEM). The results demonstrate that the average temperature and VOF-PCM, AV-MO concentration, and AV-MO temperature are enhanced from morning to noon and decreased from noon to evening. An increment in the thickness of PCM causes the VOF-PCM in desalination water to reduce by 35%. An enhancement in the glass angle reduces the average temperature of PCM, especially in the morning and afternoon. The change in PCM thickness, especially in the evening, significantly enhances the AV-MO temperature.

1. Introduction

Water is the origin of life for all creatures in the world. Some factors, such as population growth and human requirements, are continuously reducing the water consumption percentage. Water quality also changes due to human activities and the entry of various pollutants, ultimately affecting human health [1–3]. The history of human life indicates that in addition to trying to find water sources, humans have always attempted to ensure its proper quality, for example, the storage of water in copper and silver containers, the use of sunlight to improve the properties of water, storage, and boiling, the use of sand and gravel beds, which lead to the utilization of many advanced water purification processes [4]. Water is a vital element with specific characteristics. It is one of the most important chemical elements. Most arid and semi-arid countries are facing problems caused by the lack of water suitable for natural applications [5]. Desalination of seawater has quickly become a massive source of drinking water production in many regions of the world [6]. The desalination process is a process to purify sea water for drinking [7,8]. The desalination process leads to the purification of salt water and the removal of salt from the water [9,10]. Aybar [11] introduced seawater into sealed shallow tanks. A transparent cover such as

* Corresponding author. Department of Mechanical and Aeronautical Engineering, University of Pretoria, South Africa.
** Corresponding author. Mechanical Engineering Department, College of Engineering, Najran University, P.O. Box (1988), Najran, 61441, Saudi Arabia.
E-mail addresses: jmmustafa@nu.edu.sa (J. Mustafa), mohsen.sharifpur@up.ac.za (M. Sharifpur).

https://doi.org/10.1016/j.csite.2023.103357
Received 2 May 2023; Received in revised form 19 July 2023; Accepted 30 July 2023
Available online 31 July 2023

glass or plastic covered the upper surface of the device. The water in the pond was heated as the solar radiation smashed into it through the glass. The glass decreased convectional heat loss and stopped radiation from leaving the device's chamber. As a result, the distillation apparatus's thermal energy buildup raised the temperature of the water and the chamber, which in turn increased the volume of water vapor inside. The water vapor condensed on the inner surface of the glass due to heat transfer from the glass to the environment as the relative humidity in the chamber gradually increased, and the clean water resulting flowed to the water collection components at the bottom of the glass cover. Additionally, the system intermittently or permanently removed condensed salt water. Mousa et al. [12] evaluated the performance of humidification-dehumidification processes with different carrier gases by modeling and simulation methods. The carrier gases used in this performance assessment, in addition to air, included hydrogen, helium, neon, nitrogen, oxygen, argon, and carbon dioxide. The findings showed that while argon and carbon dioxide provide a better mass flux than air, hydrogen and helium have more heat flux. Due to its mass and heat flux, carbon dioxide was suggested as a carrier gas in desalination systems based on the humidification-dehumidification principle. A numerical and experimental study on the humidification-dehumidification process using solar energy in the weather of Suez city, Egypt, was carried out by Nafey et al. [13] and Nafey et al. [14]. The efficiency of the system is strongly influenced by the temperature of the salt water entering the evaporator, according to both numerical and experimental results. The efficiency of the system was hardly affected by the flow rate of condenser cooling water, air flow rate, solar radiation intensity, wind speed, or ambient temperature. According to the literature review, the need for desalinated water is felt with the increase in water demand and the scarcity of water resources [15]. Besides, the issue of energy consumption and its effects on the environment will increase significantly [16]. Therefore, in desalination technologies, the energy and the amount of water demand should be fully considered. One of the best uses of renewable energy is the desalination process, which uses solar energy [17]. It is appropriate to use solar energy for desalination in remote areas. The amount of solar radiation varies globally, with the equator receiving the most of it. This article uses SOST for three-dimensional simulations, a PCM for the desalinated water tank, and nanoparticles for the water itself. The variables of the problem include the HTFC on the glass, the PCM thickness, and the angle of the desalination glass. By changing these parameters, the melting process in the PCM and its temperature, moisture temperature, and moisture concentration are evaluated. The innovations of the present work are the use of PCM and two-phase nanofluid in SOST and three-dimensional analysis of the process.

2. Problem definition

The geometry of the SOST is illustrated in Fig. 1. It has two glasses for the passage of solar irradiation. The angle of one of these glasses varies from 10 to 45° (θ). The HTFC (h) on the glass is also varied from 5 to 300 W/m^{2}K. The PCM is used at the bottom of the desalination, and its thickness (LPCM) is varied from 10 to 50 mm. Aluminum nanoparticles with a volume fraction of 0.1% are suspended in the water in the desalination. The properties of nanoparticles, water, and PCM are presented in Table 1. The side walls of the SOST are insulated, and non-uniform solar heat flux is applied to it in 12 h.

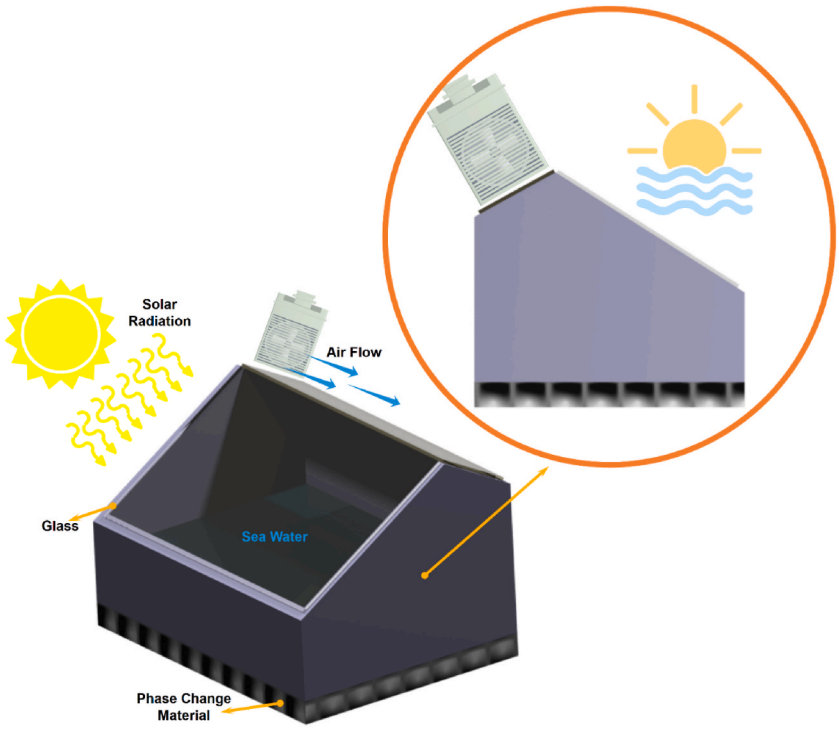

Fig. 1. A schematic of the SOST.

3. Governing equations and numerical method

The equations used to solve the flow in the SOST are as follows [19]:

$$\frac{\partial u}{\partial x}+\frac{\partial u}{\partial y}+\frac{\partial w}{\partial z}=0 \tag{1}$$

$$\rho\left[u\frac{\partial u}{\partial x}+v\frac{\partial u}{\partial y}+w\frac{\partial u}{\partial z}\right]=-\frac{\partial p}{\partial x}+\mu\left[\frac{\partial^2 u}{\partial x^2}+\frac{\partial^2 u}{\partial y^2}+\frac{\partial^2 u}{\partial z^2}\right] \tag{2}$$

$$\rho\left[u\frac{\partial v}{\partial x}+v\frac{\partial v}{\partial y}+w\frac{\partial v}{\partial z}\right]=-\frac{\partial p}{\partial y}+\mu\left[\frac{\partial^2 v}{\partial x^2}+\frac{\partial^2 v}{\partial y^2}+\frac{\partial^2 v}{\partial z^2}\right]+\beta g(T-T_0)+\beta^* g(C-C_0) \tag{3}$$

$$\left[u\frac{\partial T}{\partial x}+v\frac{\partial T}{\partial y}+w\frac{\partial T}{\partial z}\right]=\alpha\left[\frac{\partial^2 T}{\partial x^2}+\frac{\partial^2 T}{\partial y^2}+\frac{\partial^2 T}{\partial z^2}\right] \tag{4}$$

$$\left[u\frac{\partial C}{\partial x}+v\frac{\partial C}{\partial y}+w\frac{\partial C}{\partial z}\right]=D_{AB}\left[\frac{\partial^2 C}{\partial x^2}+\frac{\partial^2 C}{\partial y^2}+\frac{\partial^2 C}{\partial z^2}\right] \tag{5}$$

The two-phase mixture model is used to solve the nanofluid flow, which is given as:

$$\nabla\cdot\left(\rho_m\vec{V}_m\right)=0 \tag{6}$$

$$\nabla\cdot\left(\rho_m\vec{V}_m\vec{V}_m\right)=-\nabla P_m+\nabla.\left(\mu_m\nabla\vec{V}_m\right)+\nabla.\left(\sum_{k=1}^{n}\varphi_k\rho_k\vec{V}_{dr,k}\vec{V}_{dr,k}\right) \tag{7}$$

$$\nabla.\sum_{k=1}^{n}\left(\varphi_k\vec{V}_k(\rho_k H_k+p)\right)=\nabla.(k_m\nabla T) \tag{8}$$

$$\nabla.\left(\varphi_p\rho_p\vec{V}_m\right)=-\nabla.\left(\varphi_p\rho_p\vec{V}_{dr,p}\right) \tag{9}$$

$$\vec{V}_m=\frac{\sum_{k=1}^{n}\varphi_k\rho_k\vec{V}_k}{\rho_m} \tag{10}$$

$$\rho_m=\sum_{k=1}^{n}\varphi_k\rho_k \tag{11}$$

$$\begin{aligned}\mu_m&=\frac{\mu_f}{(1-\varphi)^{2.5}}\\ k_m&=\left\{\frac{k_p+2k_f-2\varphi(k_f-k_p)}{k_p+2k_f+\varphi(k_f-k_p)}\right\}k_f\end{aligned} \tag{12}$$

k_m and μ_m represent the coefficient of thermal conductivity and viscosity, respectively [20,21].

Table 1
The thermophysical properties of the base flow and nanoparticles [18].

Thermophysical properties	n-Eicosane	Al	Water
Pr	-	-	6.2
$C_p\left(\frac{J}{kgK}\right)$	2040 (Liquid) 2010 (Solid)	765	4179
$k\left(\frac{W}{mK}\right)$	0.15	40	0.613
$\rho\left(\frac{kg}{m^3}\right)$	856 (Liquid) 758 (Solid)	3970	997.1
$\mu\left(\frac{kg}{m.s}\right)$	-	-	8.9×10^{-4}
$T_m(^{\circ}C)$	29	-	-
$\lambda(kJ/kg)$	241	-	-

$$H_k = h_k - \frac{P}{\rho_k} + \frac{v_K^2}{2} \tag{13}$$

$$\overrightarrow{V}_{dr,k} = \overrightarrow{V}_k - \overrightarrow{V}_m \tag{14}$$

$$\overrightarrow{V}_{pf} = \overrightarrow{V}_p - \overrightarrow{V}_f \tag{15}$$

$$\overrightarrow{V}_{dr,p} = \overrightarrow{V}_{pf} - \sum_{k=1}^{n} \frac{\varphi_k \rho_k}{\rho_m} \overrightarrow{V}_{fk} \tag{16}$$

$$\overrightarrow{v}_{pf} = \frac{\rho_P d_p^2}{18\mu_m f_{drag}} \frac{(\rho_P - \rho_m)}{\rho_P} \overrightarrow{a} \tag{17}$$

$$f_{drag} = \begin{cases} 1 + 0.15 \quad Re_p^{0.687} & Re_P \leq 1000 \\ 0.0183 Re_P & Re_P \geq 1000 \end{cases} \tag{18}$$

The relations related to the melting process of PCM are [20,22,23]:

$$\rho \frac{\partial \overrightarrow{u}}{\partial t} + \rho(\overrightarrow{u}.\nabla)\overrightarrow{u} - \left[\frac{\mu_{PCM}}{(1-\varphi)^{2.5}}\right].\nabla^2 \overrightarrow{u} = -\nabla P + \overrightarrow{F}_b + \overrightarrow{F}_a \tag{19}$$

$$\overrightarrow{F}_b = -\rho_{liquid}(1 - \beta(T - T_m))\overrightarrow{g} \tag{20}$$

$$\overrightarrow{F}_a = -\left[\frac{C(1-B(T))^2}{\left(B^3(T)+q\right)}\right].\overrightarrow{u} \tag{21}$$

$$\overrightarrow{u} = -\frac{K}{\mu}\nabla P \tag{22}$$

$$B(T) = \begin{cases} 0, T < \quad (T_m - \Delta T) \\ \dfrac{(T - T_m + \Delta T)}{(2\Delta T)}, (T_m - \Delta T) \leq T < (T_m + \Delta T) \\ 1, T \geq (T_m + \Delta T) \end{cases} \tag{23}$$

The simulations made with COMSOL software employ FEM. To simulate nanofluid flow, a two-phase mixture model is used. For the runs that take between 25 and 30 h, an internal code is used.

4. Grid study and validation

The generation of the grid on the SOST is also done using COMSOL software, Finer or coarser grids are employed according to the importance of different parts in terms of heat or meshing speed. The grid generation on the glass is extremely fine due to its very small dimensions. Also, the mesh is extremely fine in the PCM layer due to its importance. The number of elements used on the SOST and the results for the average temperature of the PCM and its VOF-PCM at 6 h are shown in Table 2. The grid with 2127000 elements is chosen for the simulations based on these findings.

To validate the present results, a similar work performed by Esfe and Toghraie [19] is utilized. They simulated SOST in three dimensions. Table 3 presents the values of the productivity rate for different hours obtained from this work and those reported by Esfe and Toghraie [19], indicating a slight difference between the results and the acceptability of the present simulations (Max error 2.1%).

5. Results and discussion

Fig. 2 illustrates the air and vapor velocity contours inside the SOST at two glass angles of 10 and 45°, the HTFC of 5 and 300 W/m^{2}K, and the PCM thickness of 10 and 50 mm. The changes in air and vapor velocity in the tank show which parts have the maximum vapor velocity and which parts have the minimum velocity. The changes in the vapor velocity in the tank are dependent on the dimensions of the SOST. The angle of the glass changes the dimensions of the SOST, and as a result, significant changes are observed in

Table 2
The number of elements of the grids generated on the SOST and their effect on T-PCM and its VOF-PCM.

No. of elements	1497000	1738000	2127000	2561000
T_{PCM}	319.81	318.55	318.39	318.38
% PCM	40.55	39.68	39.30	39.30

Table 3
Productivity rate values for different hours: a comparison between the present results and those reported by Esfe and Toghraie [19].

Time	9	11	13	15
Esfe and Toghraie [19]	-4.75	-8.73	-8.03	-3.34
Present work	-4.81	-8.81	-7.92	-3.27
% Err	1.2	0.9	1.4	2.1

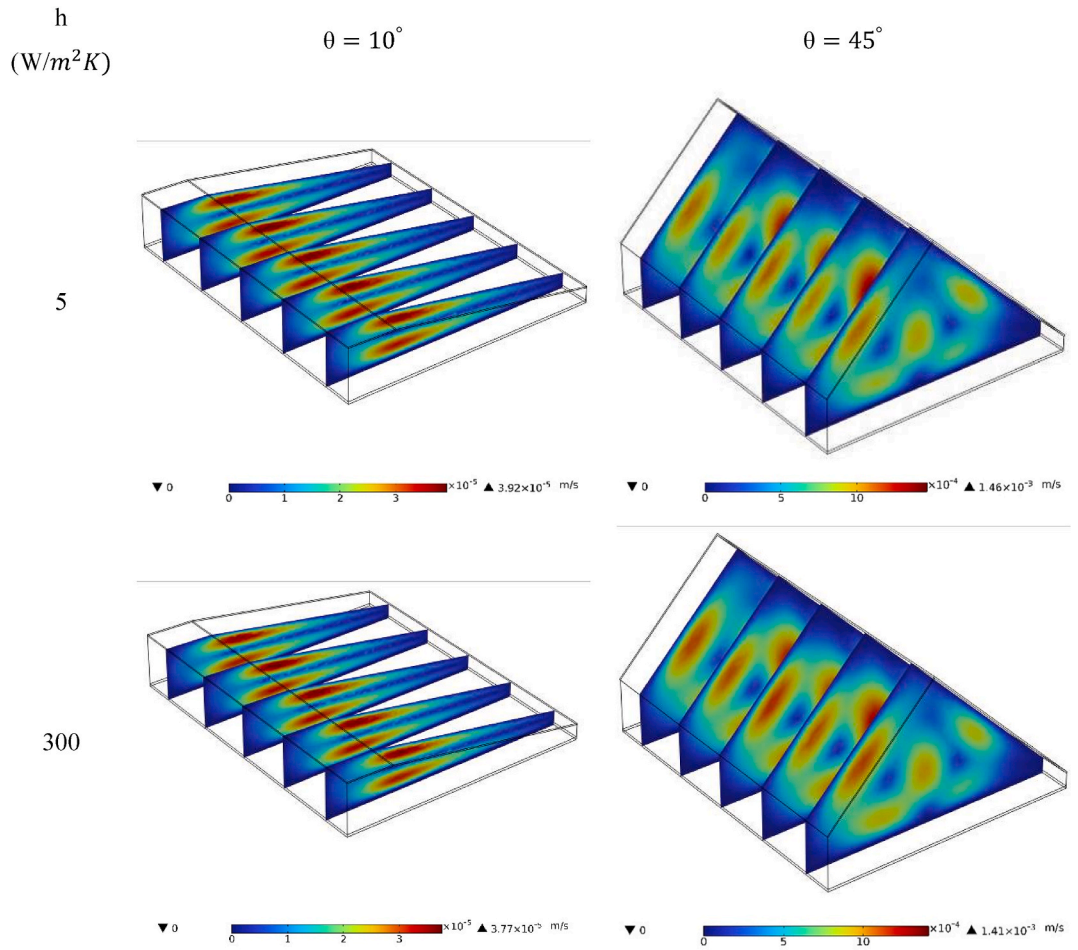

Fig. 2. The air and vapor velocity contours inside the SOST at two glass angles of 10 and 45°, the HTFC of 5 and 300 W/m^{2}K, and the PCM thickness of 10 and 50 mm.

the shape of the vortices inside the SOST. The creation of vortices is generally due to the buoyancy force created in the chamber. This force is the result of the fluid temperature difference in the SOST. At a low angle of the glass, the velocity is high on the bottom wall and top glass. However, increasing the angle of the glass changes the values of the velocity and the location of its maximum value. The enlargement of the SOST makes it easier for the fluid to move through it. Hence, it has a higher velocity. PCM thickness and HTFC have little effect on the fluid velocity in the SOST. Since the fluid movement is due to the heat transfer on the glass and the heating of the bottom wall of the SOST, any change in the temperature of these parts can have a transient effect on the fluid velocity.

Fig. 3 depicts the air and vapor temperature contours inside the SOST at two glass angles of 10 and 45°, the HTFC of 5 and 300 W/m^{2}K, and the PCM thickness of 10 and 50 mm. Due to the solar radiation on the bottom of the tank, the temperature in this area is higher and the fluid temperature is enhanced since it is in contact with the PCM at the bottom of the chamber. On the other hand, due to the contact of the glass with the ambient air, the temperature of the glass is low. When the vapor collides with the glass, the temperature of the vapor is decreased, leading to water condensation on the glass. Therefore, the temperature of the vapor at the bottom of the tank is high. It is lower at the bottom of the SOST. For low angles of the glass, the different temperature layers of vapor are placed on top of each other in a regular manner, which is due to the low velocity of the vapor in the SOST. On the other hand, at high angles of the glass, the vapor rises from the middle of the tank and moves towards the glass, and there is turbulence in the vapor.

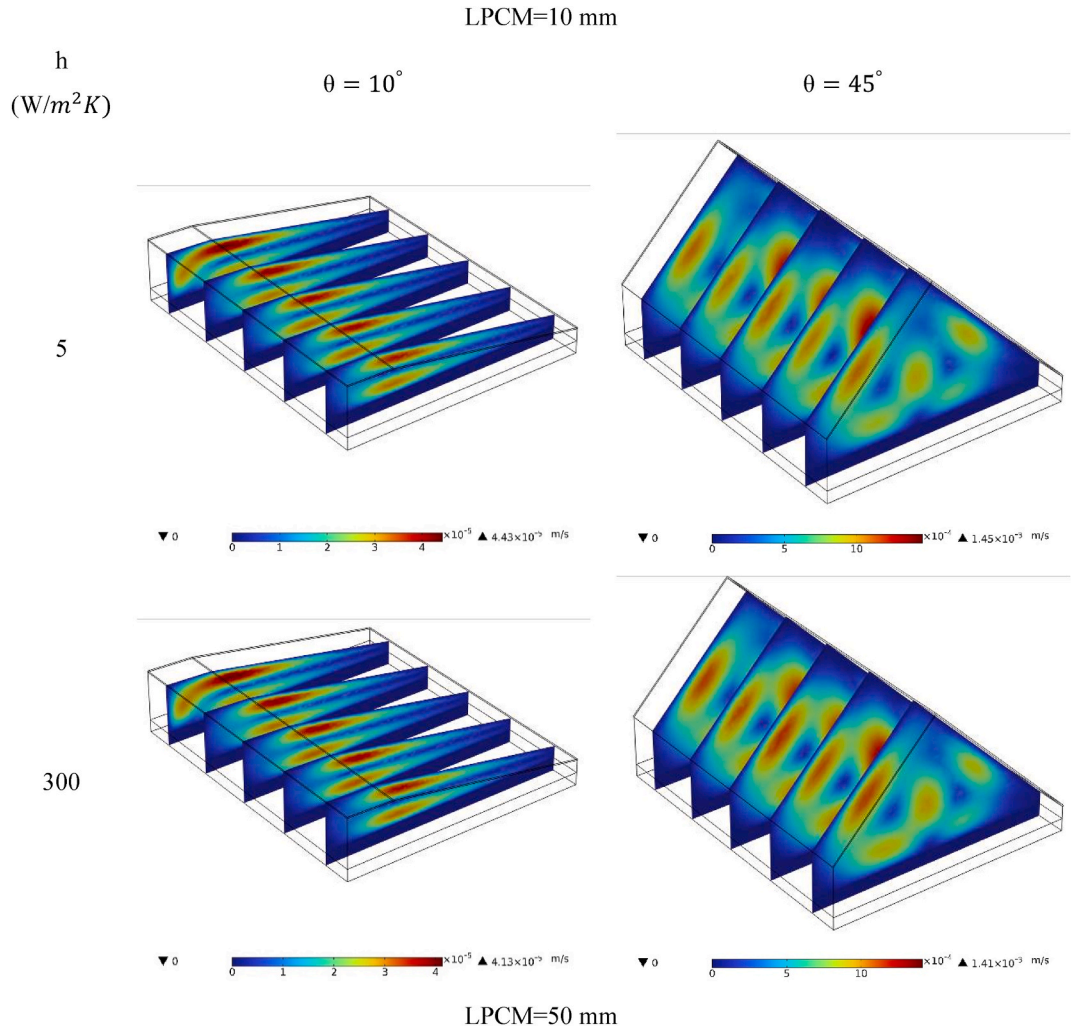

Fig. 2. (*continued*).

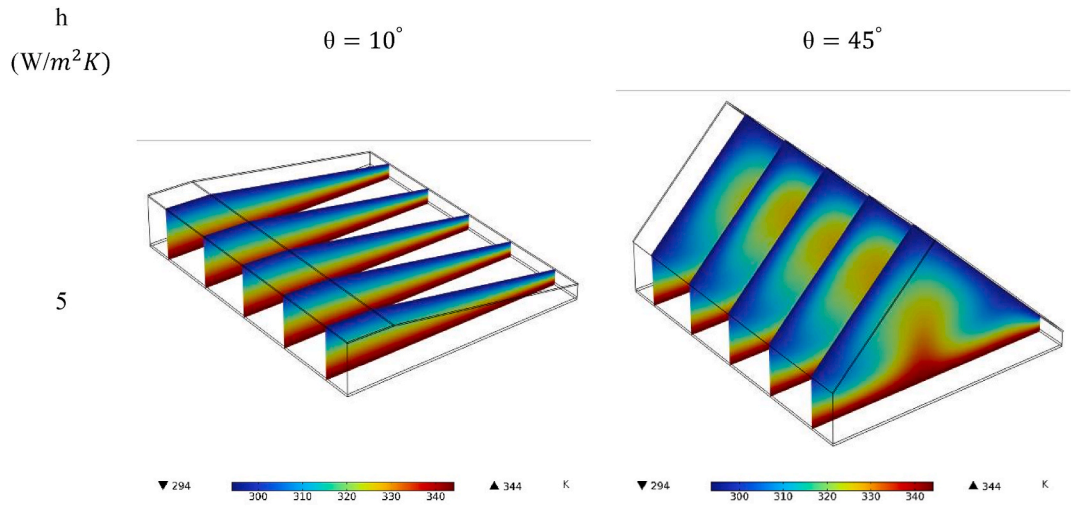

Fig. 3. The air and vapor temperature contours inside the SOST at two glass angles of 10 and 45º, the HTFC of 5 and 300 W/m^{2}K, and the PCM thickness of 10 and 50 mm.

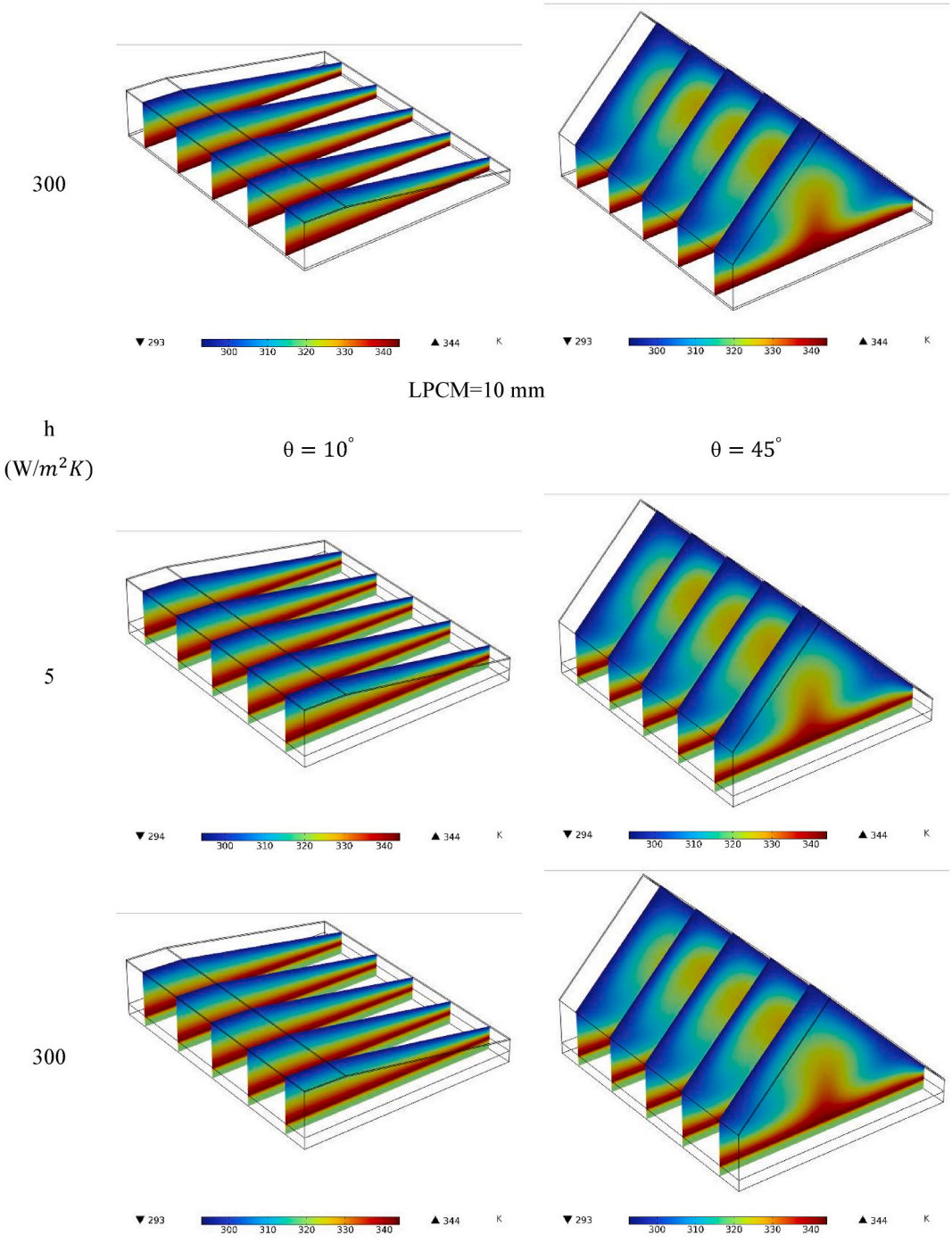

Fig. 3. (*continued*).

This is due to the higher velocity of the fluid due to the higher buoyancy force. In the part where the PCM is placed under the tank, the temperature of this part is almost constant, which is due to the PCM latent energy of melting. The enhancement in the HTFC on the glass reduces the value of the minimum temperature in the SOST due to the better heat transfer of the ambient air with the glass, resulting in a reduction in the vapor temperature near the glass.

Fig. 4 demonstrates the relative humidity contours inside the SOST at two glass angles of 10 and 45°, the HTFC of 5 and 300 W/m^{2}K, and the PCM thickness of 10 and 50 mm. The relative humidity in the SOST is changed according to the angle of the glass and the HTFC,

as well as the thickness of the PCM. The moisture rises from the water at the bottom of the tank until it reaches the cold glass, where the moisture remains on the glass as water droplets. At the top of the tank, the relative humidity is higher due to the lower temperature. The accumulation of moisture in this region causes the relative humidity to rise. Changes in relative humidity in the tank are dependent on changes in temperature and velocity of vapor. From the part where the hot vapor moves up, humidity changes can be observed. The maximum amount of relative humidity is on the glasses. Changes in the angle of the glass cause moisture to rise from the middle of the tank toward the glass and reach the glass in the upper part of the tank.

Fig. 5 illustrates the AV-MO concentration in 12 h for different angles of the glass, different values of the HTFC, and different thicknesses of PCM. The amount of moisture in the SOST is very important and is effective on the amount of freshwater produced in it.

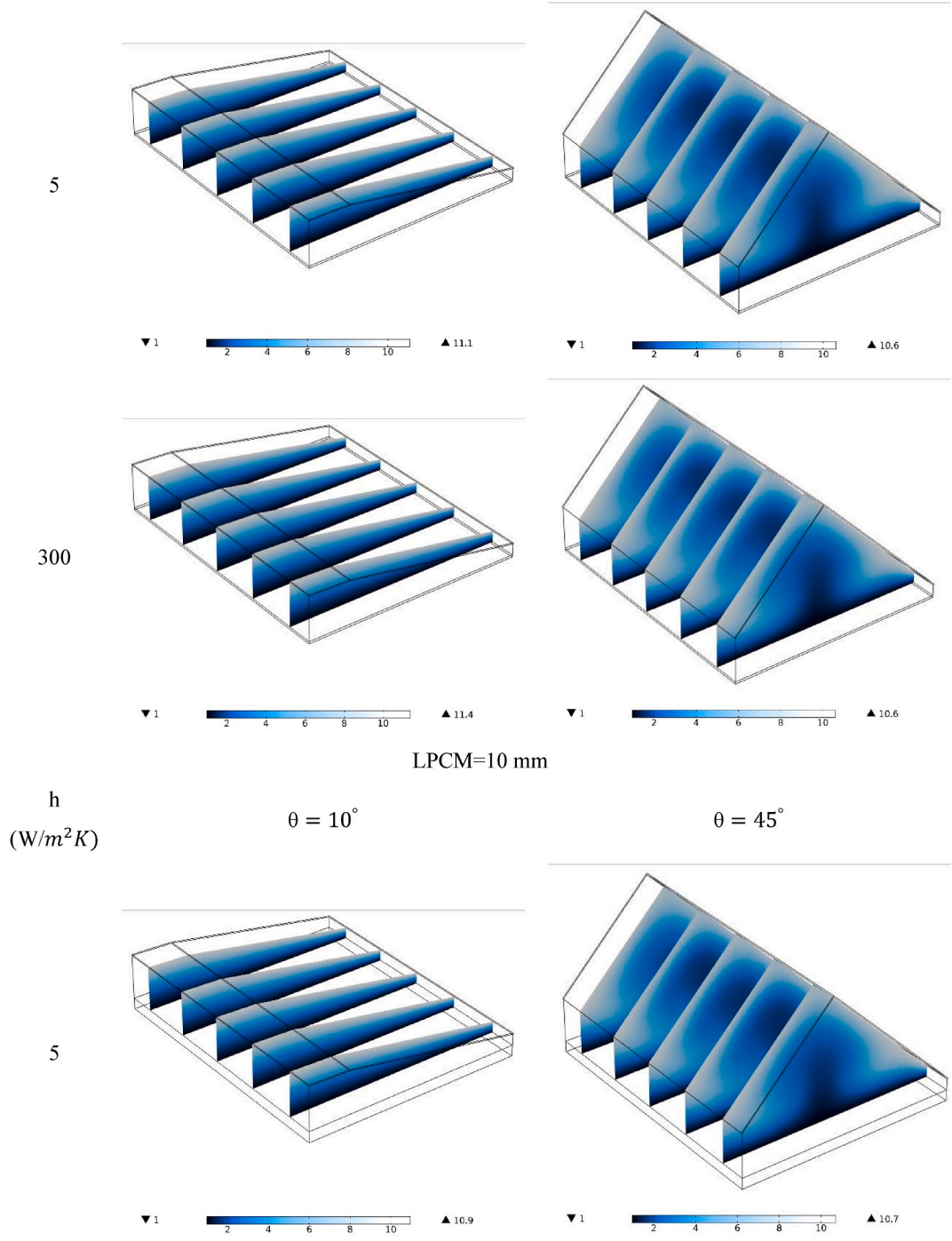

Fig. 4. The relative humidity contours inside the SOST at two glass angles of 10 and 45°, the HTFC of 5 and 300 W/m^{2}K, and the PCM thickness of 10 and 50 mm.

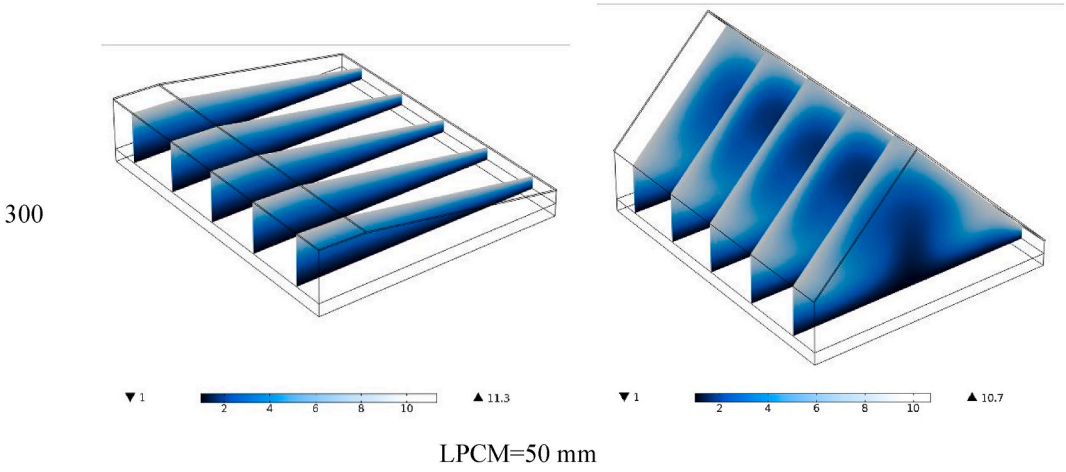

Fig. 4. (*continued*).

The changes in this parameter are dependent on the amount of solar heat flux and the time, which indicates the change in solar flux. The AV-MO concentration is maximal in the afternoon when the maximum amount of solar irradiation is received by the SOST. It can be seen that the presence of PCM leads to the maximum value of AV-MO concentration occurring in the afternoon. The presence of PCM at the bottom of the tank results in energy storage during the hours when the solar energy is maximal. Part of the energy is spent on changing the PCM phase. In the early hours of the morning, when the amount of energy received by the SOST is too low, the presence of PCM causes some of this energy to be spent on heating and changing the phase of PCM, which ultimately leads to a sharp decrease in AV-MO concentration. On the other hand, the AV-MO concentration is higher in the afternoon than that in the morning due to the energy stored in PCM. The change of the HTFC has a small effect on the AV-MO concentration, but the enhancement in the glass angle results in a reduction in the AV-MO concentration, especially during the peak hours of solar radiation. Also, the use of more PCM at the bottom of the tank leads to an increment in the AV-MO concentration in the afternoon.

Fig. 6 shows the average temperature of moisture in 12 h for different angles of the glass, different values of the HTFC, and different thicknesses of PCM. Enhancing the temperature in the SOST causes more vapor to be produced, which can be a desirable thing. It can be seen that during the hours when the amount of radiation received by the SOST is increased, the average temperature of moisture is enhanced, which is due to the increment of the energy received by the SOST. The glass angle and the HTFC have a very small effect on the AV-MO temperature. However, the thickness of the PCM layer leads to a significant change in the AV-MO temperature. The presence of PCM at the bottom of the tank causes the amount of energy entered into the desalination water to be spent on changing the phase of PCM in the morning. On the other hand, this energy changes the PCM phase in the afternoon when the solar heat flux becomes lower, leading to a slight enhancement in the average temperature of moisture for more hours. Therefore, the SOST works for higher hours and can continue to produce water. The AV-MO temperature shows the average temperature of the mixture of air and vapor in the SOST.

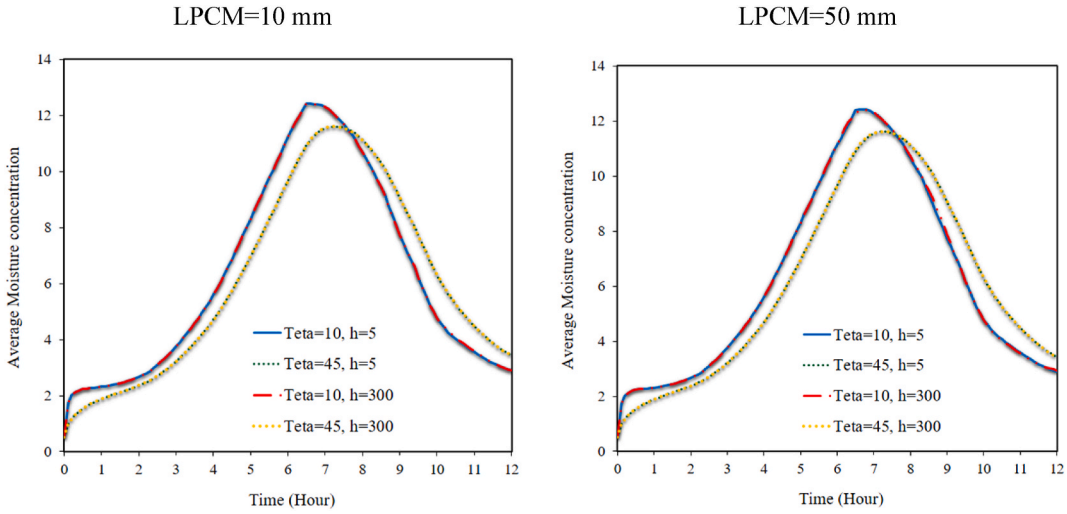

Fig. 5. The AV-MO concentration in 12 h for different angles of the glass, different values of the HTFC, and different thicknesses of PCM.

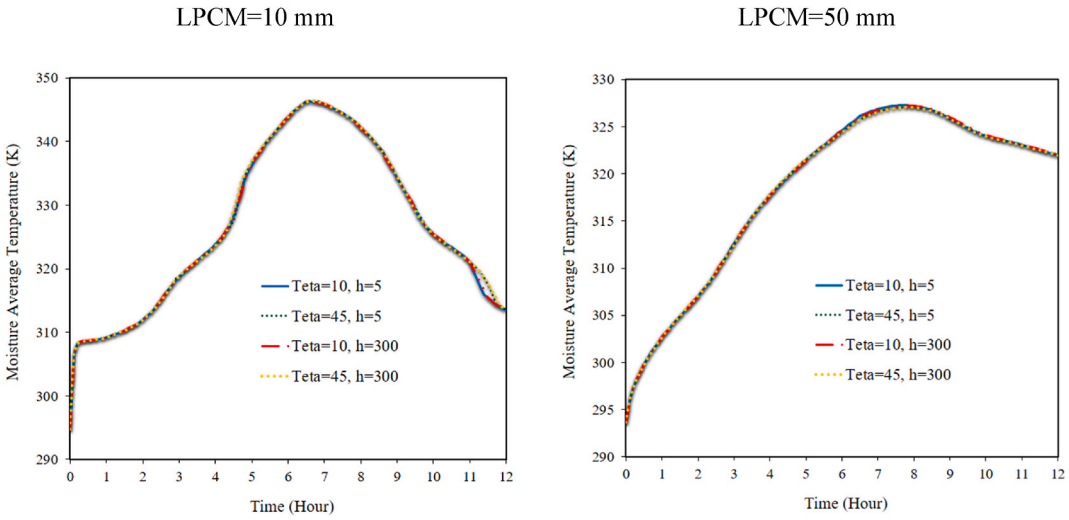

Fig. 6. The average temperature of moisture in 12 h for different angles of the glass, different values of the HTFC, and different thicknesses of PCM.

Fig. 7 demonstrates the VOF-PCM in 12 h, different values of the HTFC, different thicknesses of PCM, and different angles of the glass. The changes in the HTFC as well as the glass angle, have little effect on the VOF-PCM. In some hours, they cause a decrease or increase in the VOF-PCM. The thickness of the PCM has a significant effect on the VOF-PCM. It can be seen that the increase in the thickness of the PCM at different hours significantly reduces the VOF-PCM. From the place where the solar irradiation is received by the PCM, the melting process starts and reaches the lower regions. For small thicknesses of PCM, the PCM is completely melted in a short time due to the small volume of PCM used. All the PCM remains melted in the afternoon. In the early hours of the morning, when the radiation is weak, the T-PCM is increased, but it does not melt until its temperature reaches its melting temperature. After this time, the melting process continues depending on the thickness of the PCM. In the evening, when the solar energy is weakened again, the energy inside the PCM is transferred to the water as latent heat of fusion. If the PCM is thick, some of the PCM always remains solid and does not melt. Also, at the end of the 12 h, there is still some molten PCM in the tank, which means that the effectiveness of the SOST works even hours after the reduction of solar radiation.

Fig. 8 depicts the average temperature of PCM for 12 h for different angles of glass, different values of HTFC, and different thicknesses of PCM. The average temperature of PCM is dependent on the angle of the glass, which is seen in the morning and noon. An increment in the angle of the glass causes the average temperature of PCM to decrease. The maximum impact on the T-PCM by changing the angle of the glass occurs during the hours of peak solar irradiation. The HTFC and the thickness of the PCM have little effect on the average T-PCM. In the morning, the temperature of PCM is low until it reaches the melting temperature, and some of the PCM is melted and can reach a temperature higher than its melting point. Therefore, the change in PCM thickness has a greater impact on the T-PCM in the evening hours, because there is a greater difference in the VOF-PCM for two different thicknesses of PCM. As a result, the average T-PCM is slightly different for these two cases. The presence of vapor and water on the PCM leads to slight changes in the T-PCM because water has a high specific heat capacity affecting the T-PCM.

6. Conclusions

This article simulates SOST in three dimensions. A layer of PCM with two thicknesses of 10 and 50 mm is placed at the bottom of the SOST. Aluminum nanoparticles are also used in the desalination, and the two-phase mixture scheme is employed to solve the fluid flow. By changing the angle of the glass and the HTFC, this study is done and the following results are obtained:

1 An enhancement in the angle of the glass reduces the AV-MO concentration, but the PCM thickness and the HTFC of the glass have little effect on the AV-MO concentration.
2 The average temperature, VOF-PCM, AV-MO concentration, and AV-MO temperature with time have an increasing trend from morning to noon and a decreasing trend from noon to evening.
3 The glass angle and HTFC have little effect on the AV-MO temperature, but the PCM thickness, especially in the evening, leads to a significant enhancement in the AV-MO temperature.
4 The increment in the thickness of PCM causes the VOF-PCM to reduce drastically so that the amount of molten PCM is decreased by 35% during the peak hours of radiation.
5 An enhancement in the angle of the glass causes the average temperature of PCM to reduce, especially in the morning and afternoon. An increase in the thickness of the PCM also causes the average T-PCM to enhance slightly in the evening.

Author statement

Jawed Mustafa: Supervision, Writing- Original draft preparation, Validation.

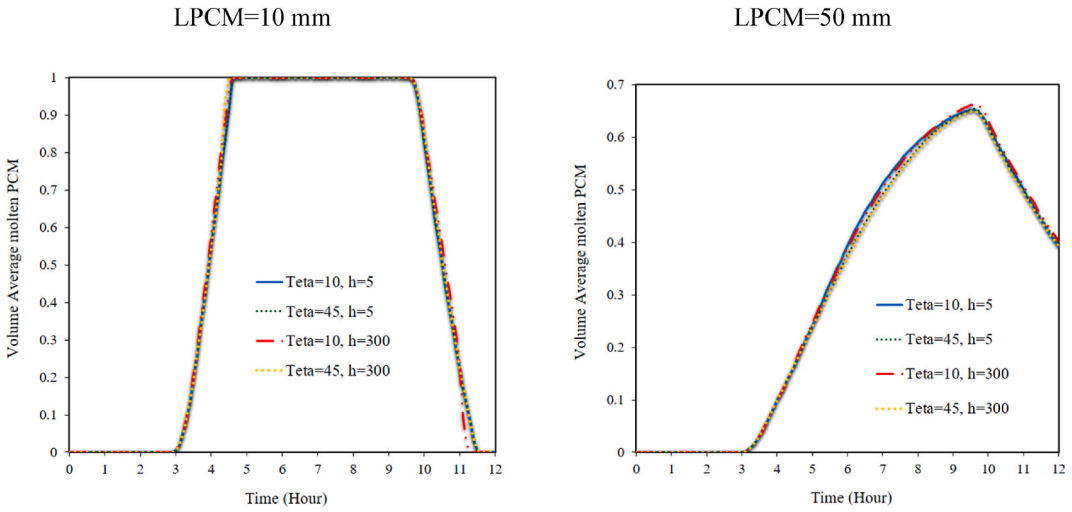

Fig. 7. The VOF-PCM in 12 h, different values of the HTFC, different thicknesses of PCM, and different angles of the glass.

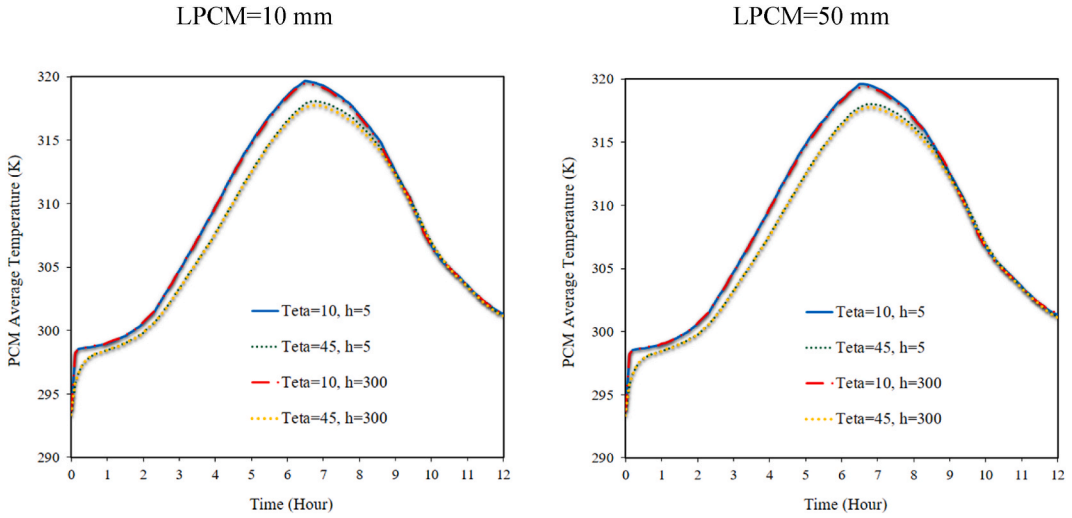

Fig. 8. The average temperature of PCM for 12 h for different angles of glass, different values of HTFC, and different thicknesses of PCM.

Saeed Alqaed: Software, Writing- Reviewing and Editing.
Mohsen Sharifpur: Writing- Reviewing and Editing, Conceptualization.

Declaration of competing interest

The authors declare that they have no known competing financial interests or personal relationships that could have appeared to influence the work reported in this paper.

Data availability

Data will be made available on request.

Acknowledgments

The authors are thankful to the Deanship of Scientific Research at Najran University for funding this work under the Research Priorities and Najran Research funding program grant code (NU/NRP/SERC/12/25).

References

[1] M.E.H. Attia, A. Karthick, A.M. Manokar, Z. Driss, A.E. Kabeel, R. Sathyamurthy, M. Sharifpur, Sustainable potable water production from conventional solar still during the winter season at Algerian dry areas: energy and exergy analysis, J. Therm. Anal. Calorim. 145 (2021) 1215–1225.

[2] J. Mustafa, S. Alqaed, R. Kalbasi, Challenging of using CuO nanoparticles in a flat plate solar collector- Energy saving in a solar-assisted hot process stream, J. Taiwan Inst. Chem. Eng. 124 (2021) 258–265.

[3] J. Mustafa, S. Alqaed, M. Sharifpur, Evaluation of energy efficiency, visualized energy, and production of environmental pollutants of a solar flat plate collector containing hybrid nanofluid, Sustain. Energy Technol. Assessments 53 (2022), 102399.

[4] A. Ejaz, H. Babar, H.M. Ali, F. Jamil, M.M. Janjua, I.M.R. Fattah, Z. Said, C. Li, Concentrated photovoltaics as light harvesters: outlook, recent progress, and challenges, Sustain. Energy Technol. Assessments 46 (2021), 101199.

[5] V.P. Katekar, S.S. Deshmukh, A review on research trends in solar still designs for domestic and industrial applications, J. Clean. Prod. 257 (2020), 120544.

[6] S.M. Alawad, R.B. Mansour, F.A. Al-Sulaiman, S. Rehman, Renewable energy systems for water desalination applications: a comprehensive review, Energy Convers. Manag. 286 (2023) 117035.

[7] R. Sathyamurthy, A.E. Kabeel, E.-S. El-Agouz, D. Rufus, H. Panchal, T. Arunkumar, A.M. Manokar, D.G.P. Winston, Experimental investigation on the effect of mgo and tio2 nanoparticles in stepped solar still, Int. J. Energy Res. 43 (2019) 3295–3305.

[8] M. Herrando, A. Ramos, J. Freeman, I. Zabalza, C.N. Markides, Technoeconomic modelling and optimisation of solar combined heat and power systems based on flat-box PVT collectors for domestic applications, Energy Convers. Manag. 175 (2018) 67–85.

[9] H.M.A. Hassan, M. Amjad, Z.u.R. Tahir, A. Qamar, F. Noor, Y. Hu, T.B. Yaqub, E.P.B. Filho, Performance analysis of nanofluid-based water desalination system using integrated solar still, flat plate and parabolic trough collectors, J. Braz. Soc. Mech. Sci. Eng. 44 (2022) 427.

[10] Z. Fu, X. Liang, Y. Li, L. Li, Q. Zhu, Performance improvement of a PVT system using a multilayer structural heat exchanger with PCMs, Renew. Energy 169 (2021) 308–317.

[11] H.Ş. Aybar, Mathematical modeling of an inclined solar water distillation system, Desalination 190 (2006) 63–70.

[12] M.K. Abu Arabi, K.V. Reddy, Performance evaluation of desalination processes based on the humidification/dehumidification cycle with different carrier gases, Desalination 156 (2003) 281–293.

[13] A.S. Nafey, H.E.S. Fath, S.O. El-Helaby, A.M. Soliman, Solar desalination using humidification dehumidification processes. Part I. A numerical investigation, Energy Convers. Manag. 45 (2004) 1243–1261.

[14] A.S. Nafey, H.E.S. Fath, S.O. El-Helaby, A. Soliman, Solar desalination using humidification–dehumidification processes. Part II. An experimental investigation, Energy Convers. Manag. 45 (2004) 1263–1277.

[15] T. Elango, A. Kannan, K. Kalidasa Murugavel, Performance study on single basin single slope solar still with different water nanofluids, Desalination 360 (2015) 45–51.

[16] L. Sahota, G.N. Tiwari, Exergoeconomic and enviroeconomic analyses of hybrid double slope solar still loaded with nanofluids, Energy Convers. Manag. 148 (2017) 413–430.

[17] D.B. Singh, G.N. Tiwari, Exergoeconomic, enviroeconomic and productivity analyses of basin type solar stills by incorporating N identical PVT compound parabolic concentrator collectors: a comparative study, Energy Convers. Manag. 135 (2017) 129–147.

[18] T. Tayebi, A.J. Chamkha, Entropy generation analysis due to MHD natural convection flow in a cavity occupied with hybrid nanofluid and equipped with a conducting hollow cylinder, J. Therm. Anal. Calorim. 139 (2020) 2165–2179.

[19] M. Hemmat Esfe, D. Toghraie, Numerical study on the effect of solar radiation intensity on the fresh water productivity of solar still equipped with Thermoelectric Cooling System (TEC) for hot and dry areas of Semnan, Case Stud. Therm. Eng. 32 (2022), 101848.

[20] H.C. Brinkman, The viscosity of concentrated suspensions and solutions, J. Chem. Phys. 20 (1952), 571-571.

[21] H.Ş. Aybar, M. Sharifpur, M.R. Azizian, M. Mehrabi, J.P. Meyer, A review of thermal conductivity models for nanofluids, Heat Tran. Eng. 36 (2015) 1085–1110.

[22] A.D. Brent, V.R. Voller, K.J. Reid, Enthalpy-porosity technique for modeling convection-diffusion phase change: application to the melting of a pure metal, Num. Heat Tran. 13 (1988) 297–318.

[23] V.R. Voller, C. Prakash, A fixed grid numerical modelling methodology for convection-diffusion mushy region phase-change problems, Int. J. Heat Mass Tran. 30 (1987) 1709–1719.